THE ASTROPHYSICAL JOURNAL, 340:117–128, 1989 May 1

SUPERLUMINAL MOTION IN THE QUASAR 3C 279

S. C. UNWIN AND M. H. COHEN
Owens Valley Radio Observatory, California Institute of Technology
J. A. BIRETTA
Harvard-Smithsonian Center for Astrophysics
AND
M. W. HODGES AND J. A. ZENSUS
Owens Valley Radio Observatory, California Institute of Technology
Received 1988 August 11; accepted 1988 September 30

ABSTRACT

VLBI maps of the quasar 3C 279 have been made at 5, 11, and 22 GHz, at several epochs between 1981 and 1985, to study the varying structure of the compact radio source. Superluminal motion is seen in two components, with apparent speed $v \approx 2.2c$ (for a Hubble constant $H_0 = 100$ km s^{-1} Mpc^{-1} and $q_0 = 0.5$), only one-quarter of the expansion rate reported in the early 1970's. The structure comprises a close double in P.A. $-135°$, seen at all three frequencies, along with steep-spectrum emission extending a few tens of parsecs (projected) and seen only at 5 GHz. The source axis points within 10° of the kiloparsec-scale jet seen by the VLA. Spectra derived from the maps show that the NE component has the highest turnover frequency, and thus probably represents the "core" of the source. By comparing the predicted inverse-Compton X-ray emission with the measured X-ray flux, we derive lower limits to the Doppler factor δ for the compact components. The core spectrum is consistent with no beaming ($\delta = 1$), but the SW component has $\delta \geq 2$, confirming the presence of bulk relativistic motion. Thus a simple model of a jet which is mildly relativistic (Lorentz factor $\gamma \geq 2$) explains both the superluminal motion and the X-ray flux.

Subject headings: interferometry — quasars — radio sources: variable

I. INTRODUCTION

The quasar 3C 279 is identified with the most compact component in an extended radio source which shows structure out to a radius of about 10″ (de Pater and Perley 1983). Its optical emission is highly variable on time scales as short as a week or less, and strongly polarized (Moore and Stockman 1981). It is also a relatively strong X-ray emitter (Zamorani *et al.* 1981). The radio structure is of the D2 class (Miley 1971), i.e., having a dominant compact component with a flat radio spectrum, and steep spectrum emission to one side of this "core." In the maps of de Pater and Perley, the core is designated "B," and "knots" in the jet of emission extending in P.A. $-145°$ are "C–G." They also detected an extended feature "A" on the opposite side of the core, which is a significant result in the light of recent discussions on the relation between large-scale and small-scale jets in quasars and radio galaxies (see discussion, § VI).

Component "B" is the VLBI source referred to as 3C 279 in this paper, one of the first objects studied with VLBI and the first in which superluminal motion was recognized (Whitney *et al.* 1971). During the early 1970's this result was confirmed by a series of observations at 7.85 GHz in which the visibility showed a sharp cusp which could be represented well by an almost-equal double. The measured expansion rate of ≈ 0.5 mas yr^{-1} along P.A. $-140°$ corresponded to an apparent separation speed of $\beta_{\rm obs} \approx 9h^{-1}$ (Cotton *et al.* 1979). But 5 GHz observations in 1974–1975 by Pauliny-Toth *et al.* (1981) did not show visibilities characteristic of a double source. Since the mid-1970's, the source received relatively little attention from VLBI observers, apparently because its unfavorable declination ($-5°$) makes it difficult to map well: the (u, v) coverage for a typical intercontinental VLBI array is very elongated, resulting in a beam profile with an axial ratio of about 8:1. More recently, Pilbratt (1986) has made 5 GHz maps with higher N–S resolution, showing structure extending to about 15 mas from the brightest peak.

This source has been widely regarded as an archetypical superluminal source, even though published observations are sparse and somewhat conflicting, and were done early in the history of VLBI. As interesting results have come from detailed monitoring of other compact sources such as 3C 120, 3C 273, 3C 345, and BL Lac, we decided to include 3C 279 in our program of VLBI monitoring, starting in 1981. This paper presents the first series of multifrequency hybrid maps of this source and discusses in more detail the preliminary results of Unwin (1987).

Throughout this paper, we use a Hubble constant $H_0 = 100h$ km s^{-1} Mpc^{-1}, and deceleration parameter $q_0 = 0.5$. For the measured redshift of $z = 0.538$ (Burbidge and Rosenburg 1965), this corresponds to a comoving coordinate distance $R = 1170h^{-1}$ Mpc, and the linear scale is 1 mas $\equiv 3.7h^{-1}$ pc. Where necessary, we have adjusted quoted distance-dependent parameters (e.g., apparent transverse velocity) from the literature to include h explicitly. Spectral index α is defined by $S \propto \nu^{\alpha}$, where S is flux density and ν is frequency.

II. VLBI OBSERVATIONS AND DATA REDUCTION

Since 1981 we have observed the core of 3C 279 at three frequencies (4.99, 10.65, and 22.23 GHz) at intervals of roughly 6 months. The sampling interval was similar for other well-studied variable sources (e.g., 3C 345 by Unwin *et al.* 1983; 3C 273 by Unwin *et al.* 1985; BL Lac by Mutel and Phillips 1987), and was chosen on the basis of previously published results on the changing structure and total flux variations (e.g.,

TABLE 1

VLBI OBSERVATIONS OF 3C 279

Epoch	Frequency (GHz)	Stations[a]	Total Flux Density (Jy)
1981.10.....	10.7	BKGFO	10.9
1981.63.....	5.0	BKGFO	12.0
1982.56.....	5.0	BKGFO	12.4
1982.92.....	22.2	KCGYO	10.5
1983.10.....	10.7	BKGFOH	12.9
1983.57.....	5.0	BKGFYO	12.9
1984.09.....	22.2	SBKNGO	8.2
1984.10.....	10.7	BKGFOH	10.0
1984.25.....	5.0	SLKGFYOHE	11.0
1984.75.....	22.2	SBKNGYO	8.5
1984.93.....	10.7	BLKGFOH	10.5
1985.61.....	10.7	LXKGFO	10.0
1985.75.....	22.2	SBKNGYO	8.7

[a] B = Max-Planck-Institut für Radioastronomie, Effelsberg, FRG (100 m); C = Algonquin Radio Observatory, Ontario, Canada (46 m); E = Hartebeesthoek Radio Observatory, Johannesburg, South Africa (26 m); F = George R. Agassiz Station, Fort Davis, TX (26 m); G = National Radio Astronomy Observatory, Green Bank, WV (43 m); H = Radio Astronomy Laboratory, University of California, Hat Creek, CA (26 m); K = Haystack Observatory, Westford, MA (37 m); L = Istituto di Radioastronomia, Medicina, Italy, (32 m); N = Naval Research Laboratory, Maryland Point, MD (26 m); O = Owens Valley Radio Observatory, Big Pine, CA (40 m); S = Onsala Space Observatory, Onsala, Sweden (26 m); X = Instituto de Pesquisas Espaciais, Atibaia, Brazil (14 m); Y = Very Large Array, National Radio Astronomy Observatory, Socorro, NM (25 m).

Andrew *et al.* 1978). Our results demonstrate that this sampling rate was in fact adequate for the motions detected. Table 1 lists the epochs, frequencies, and VLBI telescopes used in the observations. Only those telescopes which produced some useful data are listed. Also given is the total source flux density (including the extended arcsec-scale features), measured at one or more telescopes during the VLBI session.

All observations were made using the NRAO[1] Mk II System, with an effective bandwidth of 1.8 MHz, and the correlation was performed on the CIT/JPL Correlator in Pasadena. For most epochs, standard fringe-fitting with a 60 s integration time was used to determine the visibilities. We used "global" fringe fitting (Schwab and Cotton 1983) for epoch 1984.24, with results similar to those obtained with standard fitting. Calibration was also standard (Cohen *et al.* 1975), using antenna temperatures where measured, and previously determined antenna gain versus elevation curves otherwise.

For all observations except 1982.52 and 1982.92 the source was tracked continuously from horizon to horizon at a minimum of two telescopes. This is important because much of the (u, v) coverage is gained from the ends of the baseline tracks. In 1982.52 we observed 3C 279 in 20 minute scans, alternating with the nearby source 3C 273, and in 1982.92 we did the same, but with 30 minute scans. Experience gained in reducing these data led us to resume observing full tracks at later epochs, for the following reasons: (1) source switching degrades the (u, v) coverage significantly; it is already poor, due to the low source declination, which makes hybrid mapping harder. Even so, good maps were eventually made from these data. (2) In some cases, too much of each scan was devoted to pointing and system temperature calibration as each source was acquired. (3) Observing with, say, five antennas or fewer, yields too few independent closure amplitudes to allow reliable self-calibration. (4) Source structure might be missed due to significant visibility changes during the switching interval, especially if there are sharp visibility minima which would help to define component separations accurately. Apparently, though, this was not the case for 3C 279.

Hybrid maps were made from each observation using the iterative self-calibration procedure of Cornwell and Wilkinson (1981). Convergence was improved by using a reasonably accurate starting model (comprising two uniform spheres), rather than the minimal assumption of a point source. A detailed discussion of the importance of initial models in hybrid mapping is given by Biretta, Moore, and Cohen (1986). We confirmed their findings, and were able to improve upon maps made with only a point-source starting model. While use of more complicated models (three or more components) introduces an element of subjectivity into the mapping process, we are confident that the maps we present below are reliable, because (1) fits of the δ-functions of the final map to the observed data were improved, and (2) fewer obviously spurious features remained on the maps. The CLEAN window size affected the convergence only weakly. The final maps were all made with a large number of CLEAN components, and a large "window" to avoid suppressing weak extended features.

III. HYBRID MAPS

Maps were made from all the epochs listed in Table 1 and are shown in Figures 1–6. Throughout this paper, we adopt the naming convention used in several papers on superluminal sources (e.g., Unwin *et al.* 1983) by labeling the VLBI components (from west to east) as C1, C2, C3, C4, and D. Together, these comprise the (unresolved) core designated "B" on the VLA maps of de Pater and Perley (1983).

Figure 1 shows the 5 GHz maps contoured from a restoration of the CLEAN components with an elliptical Gaussian with half-power size equal to that of the "dirty" beam [because of minor variations in (u, v) coverage, an average beam size is used for convenience]. Residuals of the dirty map have not been added in, but in all cases they are much less than the lowest contour plotted. The map noise level varies between epochs, depending on the number of baseline hours observed and the calibration accuracy.

For epoch 1984.25, the observations included a southern hemisphere antenna at Hartebeesthoek, South Africa, which greatly increases the N–S resolution, and in Figure 2 we show the map from Figure 1, restored with the appropriate 0.8×1.6 mas beam. While this map should be an accurate representation of the source, some caution is required, because addition of N–S baselines breaks up the elongated "dirty" beam into a chain of roughly circular lobes (the size of the restoring beam). Because of their high level, structure with that spatial periodicity could be missed, or added spuriously. The lack of any such features, plus evidence from elsewhere on the source structure, leads us to be confident in the map of Figure 2. Biretta *et al.* (1985) have discussed similar observations of 3C 273, whose VLBI jet is unresolved transversely.

Pilbratt (1986) has made 5 GHz maps of 3C 279 at epochs, 1983.92 and 1985.40, which also included baselines to the same southern hemisphere antenna. These two maps bracket our 1984.25 map and were made independently, though with similar amounts of data, and using similar reduction tech-

[1] NRAO is operated by Associated Universities Inc., under contract with the National Science Foundation.

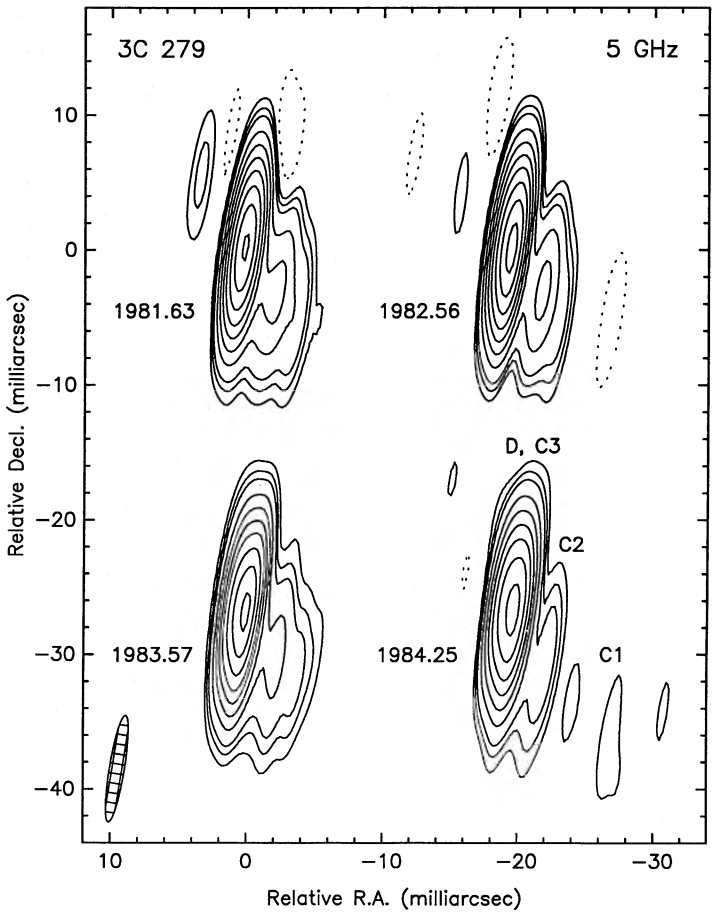

FIG. 1.—Hybrid maps of 3C 279 from four observations at 5 GHz. The restoring beam is a Gaussian with FWHM 1.1 × 8.0 mas in P.A. −9°, shown as a shaded ellipse. Contours are drawn at −0.03, 0.03, 0.06, 0.10, 0.25, 0.5, 0.9, 1.5, 2.5, 4.0, and 6.0 Jy per beam area. Components referred to in the text are identified on the last map.

niques. All three maps show an extended main "lobe" (i.e., components D and C3), and weak structure extending in roughly P.A. −140°. The high sidelobe level evidently does not affect map reliability significantly.

Figure 3 shows the 11 GHz maps, all plotted using a beam size of 0.4 × 3.2 mas. The observation of 1985.61 included the antenna at Atibaia, Brazil, which improves the N–S resolution, and in Figure 4 we show the same map plotted using the smaller (0.5 × 0.7 mas) beam. Although the map reliability is poorer [mainly because the (u, v) coverage in the N–S direction is still sparse], the source appeared unresolved transverse to its axis, to a limit of about 0.2 mas.

These 11 GHz maps show the most simple structure: a double with features of comparable brightness, with separation 1.0 to 1.5 mas in P.A. −140°. This structure also exists in the main "lobe" of emission on the 5 GHz maps, as its extension is certainly large enough to accommodate a 1.5 mas double, even though the components are blended. Only components D and C3 are visible on the 11 GHz maps (the 1981.10 map is of lower dynamic range than the others, and we believe that the third component seen there is probably an artifact). We also tried convolving the 11 GHz maps with the same beam as the 5 GHz maps for direct comparison, but the results led us to conclude that model-fitting would be a more reliable way of deriving spectral information from the two frequencies (see § V*b*).

Shorter baselines (in units of wavelengths) were observed at 5 GHz than at the higher frequencies, so more extended structure can be detected. This is the main reason why the extension to the SW which we identify as component C2 is seen only on the 5 GHz maps. Another reason may be that it has a steep spectrum ($\alpha \leq -0.7$), as the source model discussed later (§ VI) suggests. On the 1984.25 map, and in Pilbratt's (1986) maps, there is extended structure (component C1) out to at least 12 mas, in the direction of the large-scale jet.

Figure 5 shows the 22 GHz maps plotted with the same resolution as in Figure 3, for ease of comparison with the 11 GHz maps. Figure 6 shows the same data plotted with the full resolution (0.23 × 2.5 mas beam). (Epoch 1982.92 does not appear in Fig. 6, because those data lacked the long trans-atlantic baselines.) Interpretation of the 22 GHz maps is less straightforward, as the map quality is worse than at the lower frequencies. The principal structure is a clear double (components D and C3) in 1982.92 and 1984.09, but C3 apparently weakens thereafter, and a new component C4 is seen in 1985.75 closer to D (C4 is indicated in Fig. 6).

The hybrid maps presented here were used as a starting point for analysis and interpretation of the VLBI data. Because the basic structure is simple, model fitting was more appropriate for deriving quantitative results (e.g., component sizes, § VI*c*) but in all cases these were checked against the hybrid maps for consistency. We adopted this approach mainly because the poor N–S resolution of the maps makes direct

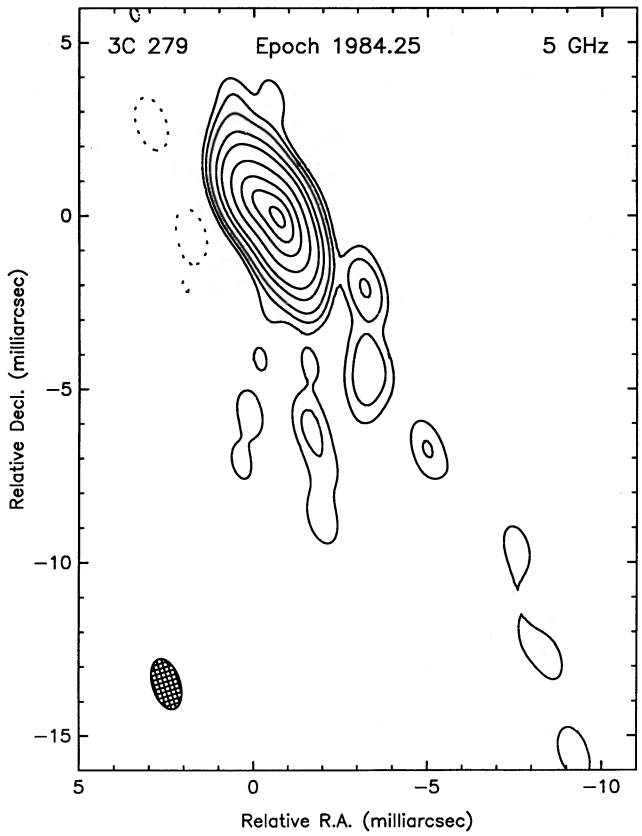

FIG. 2.—Hybrid map of 3C 279 from observations of 1984.25 at 5 GHz. This map was made from the same CLEAN components as in Fig. 1, but using a smaller restoring beam of FWHM 0.8 × 1.6 mas in P.A. 15° (see text). Contours are drawn at −0.5, 0.5, 1, 2, 5, 10, 25, 50, 75, and 95% of the peak brightness (3.4 Jy per peam area).

measurement of component positions and sizes difficult, especially when measuring along an axis which is not parallel to the minor axis of the beam.

IV. PROPER MOTION

From the series of maps in Figures 1 and 3 it is evident that there are systematic structure changes, with a time scale of roughly a year. There are a number of questions which may be asked of the observations, with regard to the changing structure: (1) do the changes represent simple expansion? (2) is the rate constant in time? (3) is the same rate found at different frequencies? (4) is there an offset in component positions between frequencies? (5) how do the results compare with measurements reported for the early 1970's?

We set out to answer these questions by a combination of model-fitting and map-measurements (see § III). The factor of 4 range in resolution meant that considerable care in the interpretation was required. For model-fitting we used two spherical components to represent D and C3, allowing the sizes and orientations to vary, which gave a very good fit to all the 11 and 22 GHz data. Some the parameters were not well constrained at 5 GHz, implying that a more sophisticated model was required.

At 5 GHz the resolution is too low to see the double structure, although expansion of the main "lobe" containing D and C3 is clearly visible. There seem to be significant changes between the three maps with high N–S resolution (our 1984.25 maps, and the 1983.92 and 1985.40 maps of Pilbratt 1986). However, the resolution along the jet is insufficient to allow component motions to be followed over such a short time base. The 22 GHz maps, up to 1984.75, also show that expansion, though the pattern clearly breaks thereafter.

In Figure 7*a* the component separations are plotted against epoch, together with $\pm 1\ \sigma$ errors derived from the model fits. The ordinate is the projection of the separation along an axis in P.A. −134°, the mean axis of the source models. Somewhat different P.A.'s found for the models made this step necessary; otherwise a one-dimensional plot would be misleading. [Another reason is that the P.A. and separation tend to be correlated, owing to the elongated (u, v) coverage.] Errors were calculated using an algorithm which examines the variation of χ^2 with each parameter. On the assumption that the structure really is double, these errors are objective measures of the uncertainty in each parameter.

There is no significant difference in the expansion rates measured at the three frequencies, though perhaps there is a slight offset between frequencies, with the 5 GHz points below the mean line, and 22 GHz points above it. Combining all the measurements shown in Figure 7*a* except those below 0.7 mas (which refer to C4), yields a proper motion $\mu = 0.12 \pm 0.02$ mas yr^{-1} with an extrapolated zero-separation epoch of 1972.6 ± 1.1. This corresponds to an apparent expansion speed of $\beta_{\rm obs} = 2.2h^{-1}$, only one quarter of the rate found by Cotton *et al.* (1979) from early 1970's data. We discuss this discrepancy further below (§ VI*b*).

The expansion between D and C3 can also be measured directly from the hybrid maps, up to about 1985.0; thereafter, C3 becomes indistinct. At 11 and 22 GHz we used the maps from Figures 3 and 5 and used the half-power point of the eastern edge of the core D as a reference point, subtracting one-half of the beam FWHM from the distance to the peak of C3. Assuming that the core is always the easternmost feature, this minimizes errors due to the blending of close-in components. At 5 GHz, we merely deconvolved the half-power width of the main lobe which contains D and C3. The results are plotted in Figure 7*b* with a fitted line $\mu = 0.11 \pm 0.04$ mas yr^{-1} and zero-separation epoch 1971.8 ± 3.5, which is formally consistent with the result from model fitting and indicates that component blending is not a serious source of bias in model-fitting. Also shown are the positions of component C2 relative to D, as measured from the maps of Figure 1. While a case for expansion cannot be made from these data alone, they are consistent with the expansion rate measured between D and C3.

V. FLUX DENSITIES AND SPECTRA OF SOURCE COMPONENTS

a) Component Flux Densities

The hybrid maps in § III contain detailed information on the flux densities of the components in the core of 3C 279, and their evolution in time. As with proper motions, extracting quantitative measurements is difficult because of the extreme beam elongation. Thus for the reasons discussed in § III we derived component flux densities by model-fitting a pair of spheres. At 11 and 22 GHz similar values could be obtained from the maps, but at 5 GHz the principal components D and C3 are blended. For consistency, we relied on the models, which generally yielded realistic formal errors.

Figure 8 shows the flux densities measured in this way, as a function of epoch. As well as formal fitting errors, there can

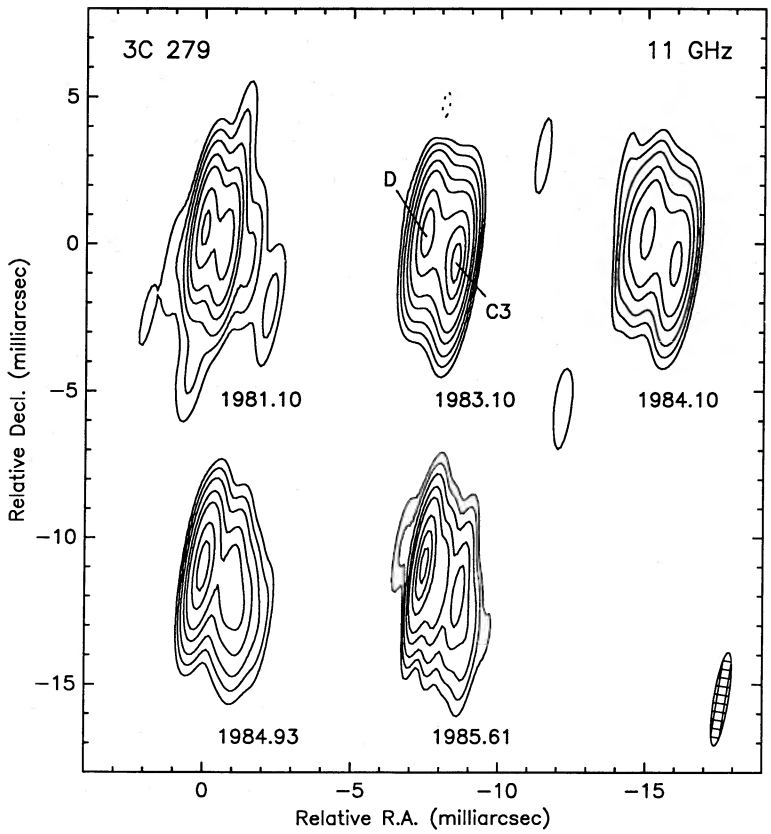

FIG. 3.—Hybrid maps of 3C 279 from five observations at 11 GHz. The restoring beam is a Gaussian with FWHM 0.5 × 3.2 mas in P.A. −9°, shown as a shaded ellipse. Contours are drawn at −0.08, 0.08, 0.16, 0.3, 0.6, 1, 2, 3, and 4 Jy per beam area.

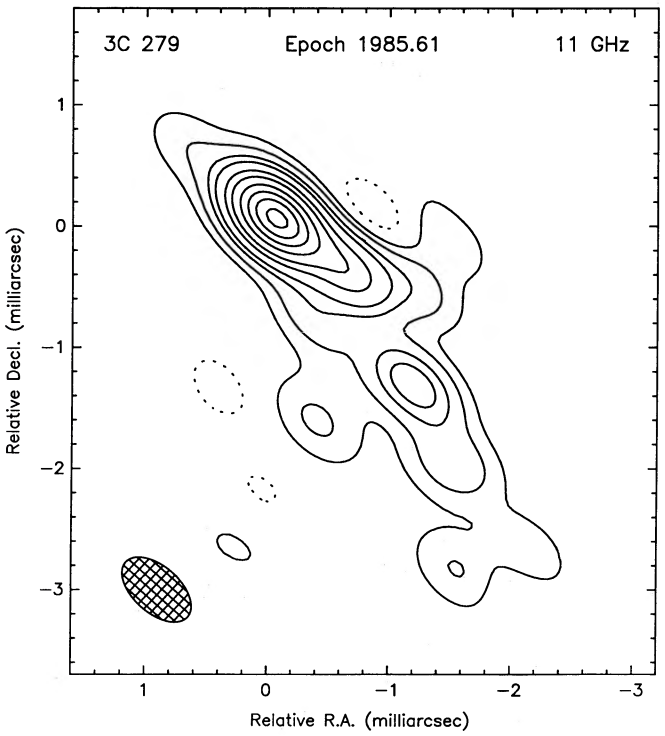

FIG. 4.—Hybrid map from observation of 1985.61 at 11 GHz. This map was made from the same CLEAN components as in Fig. 3, but using a smaller restoring beam with FWHM 0.4 × 0.7 mas in P.A. 48° (see text). Contours are drawn at −2, 2, 5, 10, 15, 25, 35, 50, 65, 80, and 95% of the peak brightness (4.2 Jy per beam area).

also be calibration errors which are independent between epochs. At 5 and 11 GHz these do not exceed 5%, but may be up to 10% at 22 GHz. Any systematic errors are not large enough to obscure the basic trends in Figure 8, which are indicated by lines drawn between the points. It is clear that a significant outburst occurred in component C3 at 5 and 11 GHz, and probably also at 22 GHz, reaching a peak around 1983.0. Meanwhile, the brightness of the core D is basically unchanged at all three frequencies.

Monitoring of the total flux density of 3C 279 by Aller *et al.* (1985) also shows an outburst peaking around 1983.0 (their monthly averages at 5, 8, and 15 GHz include linear polarization; see their Fig. 54). They measure the total source flux, which is dominated by the VLBI components, but includes the VLA jet and lobe (see § VI*a*). After making small corrections for the extended features (e.g., Aller and Olsen 1971), the total flux data show (1) components D and C3 account for all the flux of the VLA core at 5 and 11 GHz, and almost all at 22 GHz; (2) the strength of the outburst in C3 at 5 and 11 GHz agrees with the total flux outburst (and probably also at 22 GHz); (3) the timing of the outburst agrees to within about 3 months, limited only by the time range and sampling of the VLBI monitoring. We therefore conclude that most of the activity in the total flux curve during this period represents changes in C3, while the core has not varied significantly.

A detailed comparison with the total flux density variations is interesting because we can begin to relate the VLBI structure to the linear polarization measurements of Aller *et al.* (VLBI polarization mapping is currently very difficult, and has been achieved only for a few sources, e.g., Roberts and Wardle 1987). The polarization position angle of 3C 279 shows a relatively

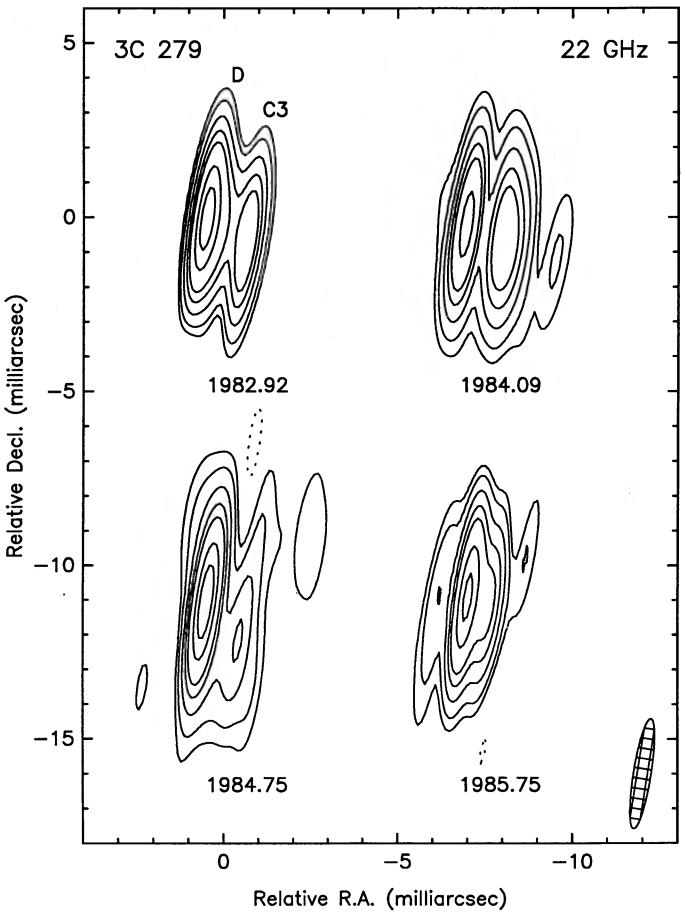

FIG. 5.—Hybrid maps of 3C 279 from four observations at 22 GHz, convolved to the resolution of the 11 GHz maps in Figure 3. Contours are drawn at −0.08, 0.08, 0.16, 0.35, 0.65, 1, 2, and 3 Jy per beam area.

simple behavior, which is perhaps unexpected, given the very large changes seen in the degree of polarization. After correcting for a constant rotation measure of $+14$ rad m^{-1} (Aller 1970), the polarization is roughly aligned with or perpendicular to the VLBI axis, with rapid swings between the two states. During the 1981–1985 outburst, the electric vector remained relatively constant within about 20° of the VLBI axis.

The polarized flux shows much larger fractional changes, and on shorter time scales than the total flux, suggesting that there is polarization activity on smaller size scales than are seen in our (unpolarized) VLBI maps. There seems to be no obvious correlation with the total flux, in which the month-to-month variations are small, or with the VLBI data, though for the latter data the time coverage is limited.

Aller, Hughes, and Aller (1987) have discussed the radio polarization and flux density variations of 3C 279 in terms of shocks propagating down a relativistic jet and causing a local ordering of the magnetic field (e.g., Hughes, Aller, and Aller 1986). Their model is remarkably successful in explaining the simultaneous behavior of the (integrated) total and polarized radio emission is sources like BL Lac and 3C 279. The basic features our VLBI maps, even without polarization information, may be incorporated into this model. We identify D as the base of the jet where it becomes optically thin and is a fairly steady source of radio emission. Components C1–C4 are regions of enhanced emission from the jet, resulting from propagating shocks with lifetimes of about a year. During 1981–1985, the total flux and polarization P.A. changes seem definitely to be related, while C3 dominates both the core and the jet components, at least at 11 GHz. Thus we may tentatively conclude that the region(s) responsible for the most of the polarized emission reside in component C3, and that the mean magnetic field is perpendicular to VLBI axis. However, there is insufficient information to extend this to include the core and its contribution to the polarized flux and P.A. In particular, the deep minimum in polarized flux at epoch 1981.7 is hard to

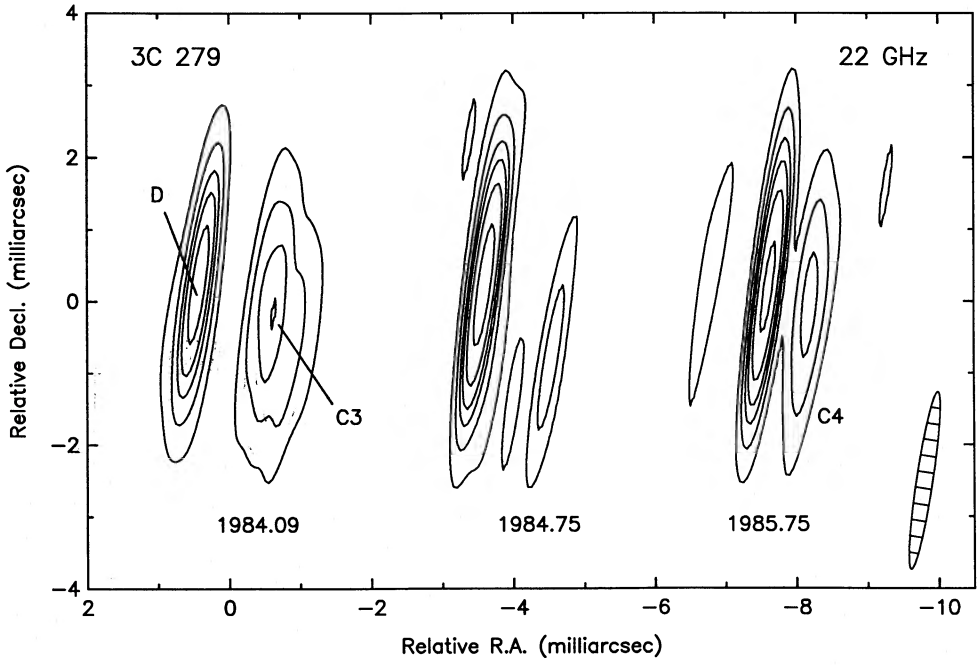

FIG. 6.—Hybrid maps of 3C 279 from three observations at 22 GHz. The maps are plotted with the full resolution of the data (beam size of 0.23 × 2.5 mas in P.A. −9°, shown as a shaded ellipse). Contours are drawn at −0.16, 0.16, 0.4, 0.7, 1.0, 1.5, and 2.5 Jy per beam area.

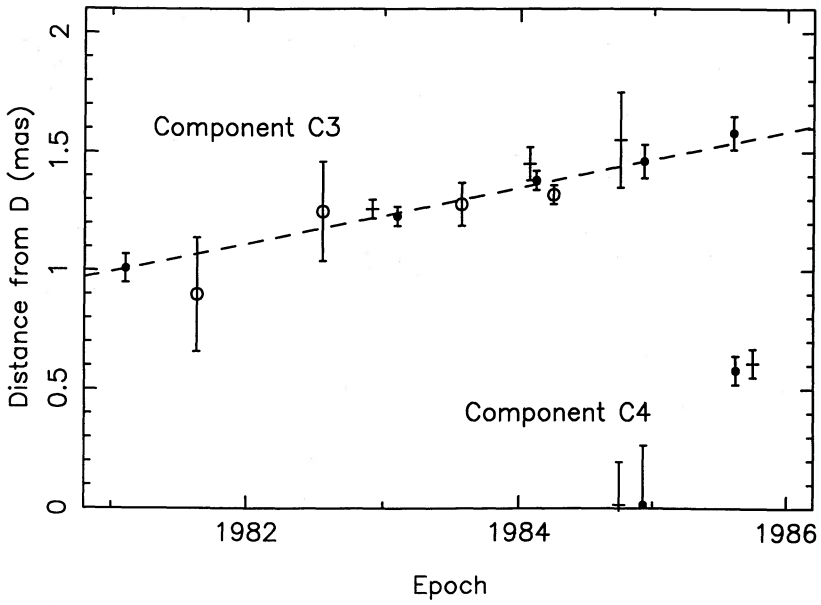

FIG. 7*a*

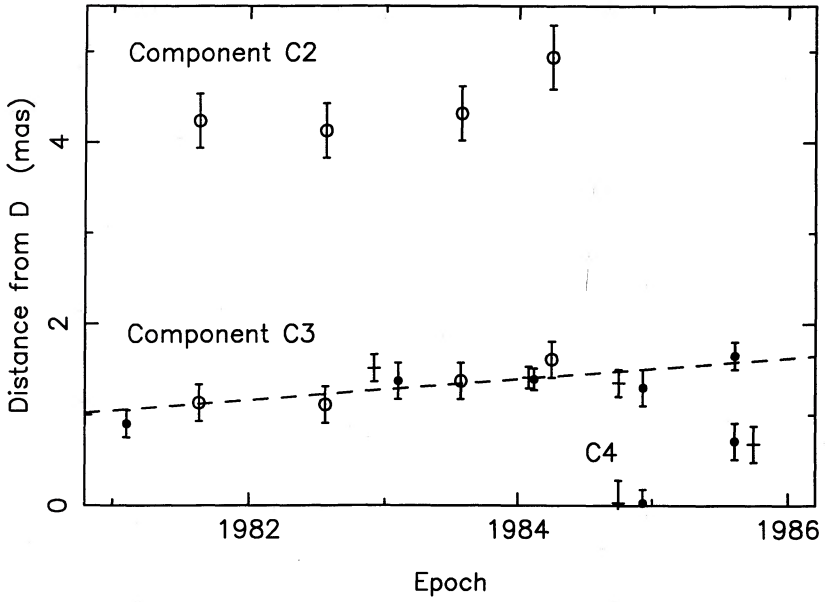

FIG. 7*b*

FIG. 7.—Component separations in 3C 279 as a function of observing (5 GHz, *open circles*; 11 GHz, *filled circles*; 22 GHz, *crosses*). (*a*) Separation between core D of 3C 279 and jet component C3 projected onto the mean axis of the models, in P.A. −134°, from model-fitting two homogeneous spheres to the visibility data. The errors shown are the formal errors from the fit. The fitted straight line has slope 0.118 mas yr^{-1} and zero-intercept at epoch 1972.56; separations below 0.7 mas refer to component C4 and were excluded from the fit (see text). (*b*) Separation of jet components C2 and C3 from core D, measured directly from the hybrid maps. The errors are estimates of uncertainties due to the resolution limit and map reliability. The fitted straight line has slope 0.116 mas per yr and zero-intercept at epoch 1972.00; separations below 0.8 mas were excluded from the fit.

reconcile with a swing in P.A. of only 30° unless there are three or more active components.

The Aller, Hughes, and Aller (1987) model predicts new shock fronts emerging from the core roughly every six months (to explain the rapid 14.5 GHz polarization outbursts) which is more often than new VLBI components are seen in unpolarized flux. The expected appearance depends on many model parameters, such as the bulk flow and shock speeds and their orientations, as well as frequency-dependent opacity and spatial resolution of the VLBI observations. This particular model with multiple shocks in quick succession leads to a blending of the components seen in unpolarized flux. If correct, this complicates the interpretation of unpolarized maps, as cautioned by Hughes, Aller, and Aller (1989), and it perhaps explains why our highest resolution 22 GHz maps show a less obvious pattern of evolution. Of course, this applies to VLBI studies of all compact sources, though the 3C 279 case is perhaps more extreme, as indicated by its very rapid changes in polarization.

An important test of the model would be to monitor the

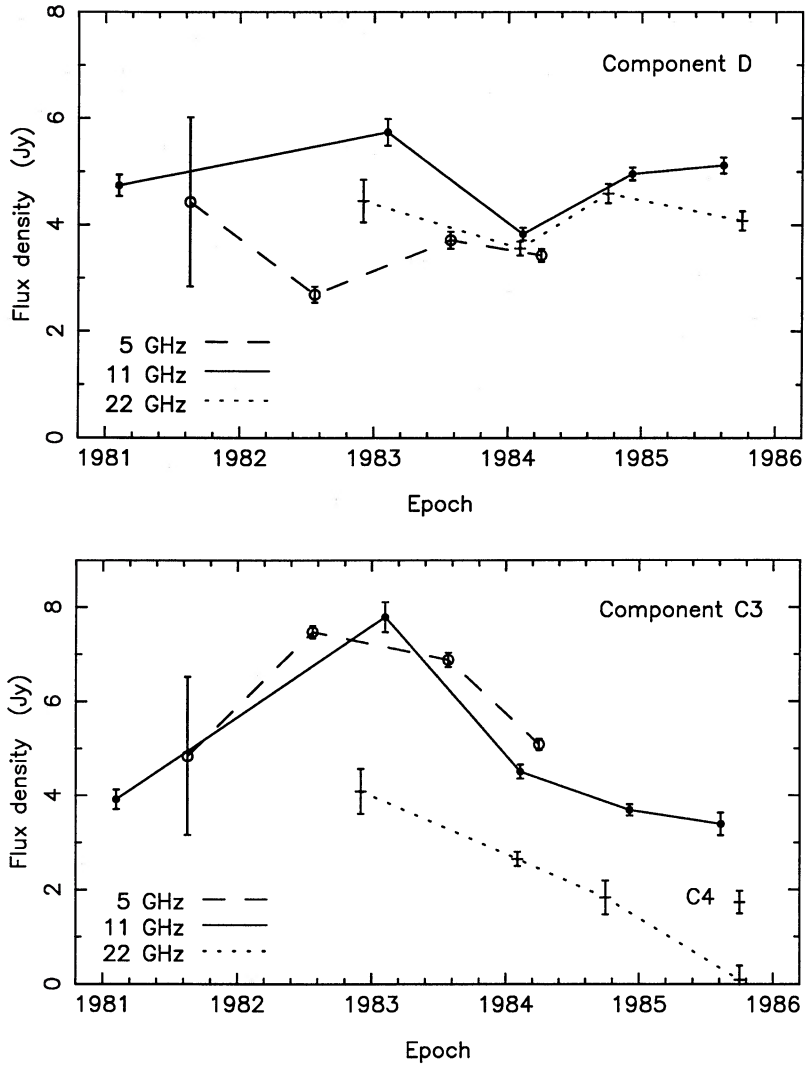

FIG. 8.—Variation of flux density as a function of observing epoch, for the core D component (*top*), and jet component C3 (*bottom*). Vertical lines represent $\pm 1\ \sigma$ formal errors from fitting homogeneous sphere models to the visibility data (see text). Symbols represent 5 GHz measurements, *open circles*; 11 GHz, *filled circles*; 22 GHz, *crosses*. For the final epoch (1985. 75) only a lower limit was found for C3; the second measurement represents a new feature C4 seen only at that epoch.

milliarcsecond spatial distribution of polarized emission, at intervals of 2 months or less, which should reveal more rapid and complicated changes than unpolarized emission. Data of this kind will be important to further constrain or refine models of the class proposed by Hughes, Aller, and Aller (1989). While not technically feasible at present, polarization monitoring would be an ideal program to undertake with the VLBA under construction by NRAO.

b) Individual Component Spectra

Radio spectra of components D and C3 may be deduced from the data in Figure 8. We evaluated the spectra at epoch 1983.10, the epoch of one of the 11 GHz maps, and interpolated data on either side of 5 and 22 GHz (there are too few data to properly follow the time-history of individual components). The results are plotted in Figure 9. Solid lines show the probable spectral shape of each component, but they are not fitted curves. Error bars are estimates which include contributions from model-fitting, calibration, and extrapolation in epoch. D and C3 account for most of the total flux, and the remainder is in structure resolved out in our observations; the amount is hard to quantify, due to uncertainties in the VLBI calibration, but it is consistent with the arcsecond-scale emission seen by de Pater and Perley (1983). Also shown in Figure 9 are measurements of the total flux density from 102.5 MHz to 859 GHz, interpolated to 1983.10 where necessary. Uncertainties in flux density variations do not significantly affect the mean curve. Landau *et al.* (1986) show a nearly-simultaneous spectrum between 1400 Å and 20 cm (for a slightly different epoch), which has essentially the same spectral shape in the radio, with the spectrum steepening smoothly into the ultraviolet.

Component D is presumably the core of 3C 279, as it has the highest turnover frequency. However, it is clearly not homogeneous, as the spectral index below 11 GHz is much flatter than the $\alpha = 2.5$ expected in the simple sphere model. This is confirmed by a study of the component angular sizes (see § VIc below): at 11 and 22 GHz, reliable size estimates were obtained, while at 5 GHz much larger sizes were found, and also larger variations between epochs. A reasonable step to take next would be to consider component D as two homogeneous subcomponents, or else a smoothly varying inhomoge-

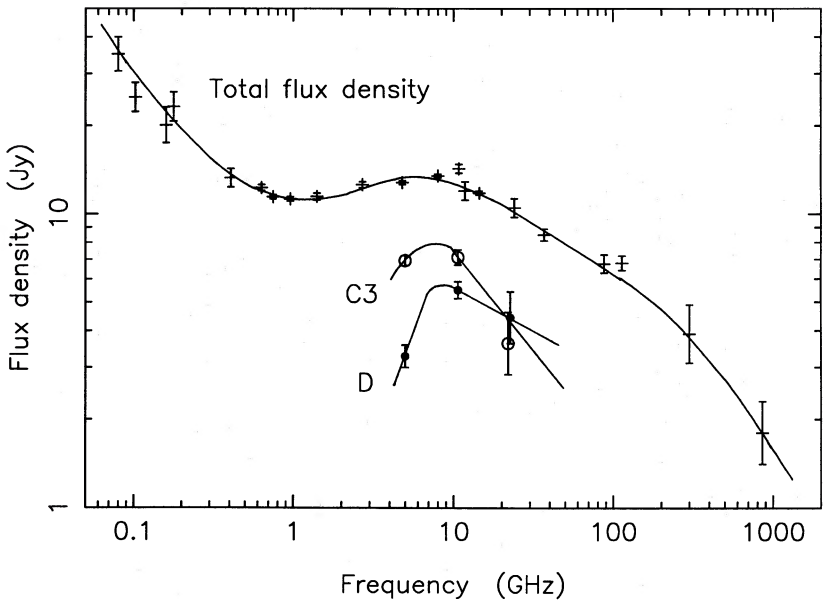

FIG. 9.—Radio spectrum of the total flux density of 3C 279 interpolated or extrapolated where necessary to epoch 1983.10. Data (in order of increasing frequency) from Vetukhnovskaya (1987); Slee and Higgins (1973); Slee (1977); Pilkington and Scott (1965); Padrielli *et al.* (1987); Wills (1975); Pauliny-Toth, Wade, and Heeschen (1966); Aller *et al.* (1985); Seielstad, Pearson, and Readhead (1983); Haddock, Aller, and Aller (1987); Salonen *et al.* (1987); G. A. Seielstad (87 GHz and 114 GHz, private communication); Roellig *et al.* (1986). Individual component spectra, derived from Fig. 8, are shown with $\pm 1\ \sigma$ estimates of the errors. The solid lines are schematic curves and are not fitted to the data.

neous jet. It would be easy to obtain agreement with the observed spectrum in this way, at the expense of adding several arbitrary parameters to the model. We note that this spectral shape is seen in other well-studied superluminal sources, such as 3C 345 (Unwin *et al.* 1983; Biretta, Moore, and Cohen 1986) and 3C 273 (Unwin *et al.* 1985). Unwin *et al.* analyzed 3C 273 in terms of the expanding jet model of Königl (1981) with reasonable agreement. The present data are consistent with one important feature of the Königl model, if component D represents the optically thick "base" of the jet, and components C3 and C2 are knots: the slight frequency dependence of the component separations (Fig. 7*a*) is in the same sense as required by the frequency-dependent opacity along the jet. Unfortunately, there is too little good VLBI data and 3C 279 to justify a detailed comparison with this class of model.

For component C3, a homogeneous synchrotron sphere model, with steep optically thin spectral index $\alpha \approx -1.0$ with a turnover between 5 and 11 GHz fits well. A measurement below 5 GHz would be required to confirm the self-absorption, but only a satellite-based experiment would have sufficient resolution to achieve this. Our identification of the spectral shape of C3 is supported by the fact that 3C 279 is so similar to the other well-studied superluminals in its (radio) spectral properties.

VI. DISCUSSION

a) Large-Scale and Small-Scale Structure

We now compare our results with the large-scale structure of 3C 279 mapped by de Pater and Perley (1983) at 5, 15, and 22 GHz. Our interpretation of the VLBI components in terms of a one-sided jet is supported by the 5 GHz VLA map, which shows several knots ("C"–"G") extending from the unresolved peak "B" in position angle $-154°$, because (1) the mean VLBI P.A. $\approx -134°$ agrees, given the limited N–S resolution, and (2) the VLBI jet points in the same sense. (From its spectrum, we identified the core to be component D, and hence C3 and C2 define the jet direction). In fact, the VLA maps show a similar distribution of component turnovers, on the arcsecond scale, namely that the turnover frequency decreases with distance from the core.

There is a large difference in scale between the maps, of course: component C2 is only 5 mas from the core, and the most distant feature is C1 at 12 mas in the 1984.25 5 GHz map. The closest VLA feature, seen in the highest resolution 22 GHz map is knot "C" at 95 mas. However, the component fluxes are of the same order: C1 is $\simeq 50$ mJy and "C" is $\simeq 25$ mJy. Although there are no data on the radio structure on intermediate scales, a continuous connection between the scales seems highly likely, as was found in 3C 120 (Walker, Benson, and Unwin 1987). Given that knots generally have normal spectra ($\alpha < 0$), components lying between 10 and 100 mas should easily be detectable in low-frequency, high dynamic range VLBI observations.

VLA monitoring of knot "C" has been started, according to de Pater and Perley (1983). It is unlikely to yield a conclusive result for many years, especially if the proper motion is closer to the present value of 0.12 mas yr^{-1} than the 0.5 mas yr^{-1} of Cotton *et al.* (1979); nevertheless, it is an important measurement to attempt.

b) Superluminal Motion

The superluminal motion ($\mu = 0.12 \pm 0.02$ mas yr^{-1}, corresponding to $\beta_{\rm obs} = 2.2h^{-1}$) measured from the present observations, covering the period 1981–1984 (§ IV) is much slower than the rate reported by Cotton *et al.* (1979) from observations in 1971–1973. Those early data, which mostly comprised single-baseline experiments, yielded $\mu = 0.5 \pm 0.1$ mas yr^{-1} from model-fitting a pair of circular Gaussians. We have reexamined the evidence of the published visibility curves, and it appears that the clear signature of a double source justifies the

simple model used to fit those data. Although it is arguable that a complicated structure could yield the same visibilities, it is certainly unnecessary, and we therefore conclude that the larger proper motion is probably correct for those early years.

A more complicated explanation of the present data is also possible, since the observations were made over larger time intervals than the early data. If we do not correctly identify the components between epochs, then the true proper motion is much higher, and our measured value is due to a "stroboscopic" effect in our sampling of the motion (e.g., Blandford 1987). We believe this to be unlikely, given the irregular sampling in time, and the fact that changes in the total flux are rather gradual (Aller *et al.* 1985). Faster variations do occur in polarized emission, as noted in § V*a*, so the spatial distribution of polarized flux density could well vary more rapidly.

The discrepancy in velocity is never likely to be properly explained, even though it appears to be real. Note that this does *not* imply a deceleration of any particular component—the Cotton *et al.* (1979) component would be about 10 mas from the core by 1984, and almost certainly too faint to be followed easily. The new lower value refers to component C3, which was prominent in the early- to mid-1980's. Pauliny-Toth *et al.* (1981) reported a proper motion of 1.1 mass yr^{-1} during 1972–1974 ($\beta_{obs} \simeq 20h^{-1}$), more than twice the large value measured by Cotton *et al.* This result was based on fitting a three-component model to very limited data, and while possibly correct, we believe it to be unreliable.

We examined the relation between the spatial evolution of the VLBI components and the history of flux density variations from Aller *et al.* (1985). The extrapolated zero-separation epoch for C3 corresponds approximately with a minor flux outburst in 1972, but since we have no direct evidence that the proper motion of C3 was constant prior to 1981, no strong conclusions can be drawn. If C3 had decelerated, then the large flux outburst in 1976 might represent the birth of this component. However, given that C3 is responsible for the peak in 1982–1983, long after its birth (§ V*a*), it is more likely that the 1976 peak is due to a flare in an older component, perhaps C2.

c) X-Ray Emission

In a source with high radio brightness and very compact (synchrotron) radio cores, significant X-ray emission via the inverse-Compton process may be detectable. It is often found that the predicted emission from quasars with VLBI cores exceeds the measured X-ray flux by several orders of magnitude. In the inverse-Compton model, an observed deficit requires bulk relativistic motion of the radio and X-ray emitting region to reduce the prediction to the observed level. This leads to a lower limit to the Doppler (blueshift) factor of the emitting material $\delta = \gamma^{-1}(1 - \beta \cos \theta)^{-1}$, where θ is the angle between the velocity vector of the moving material and the line of sight; $\beta = v/c$ is the jet speed; and $\gamma^2 = (1 - \beta^2)^{-1}$. The X-ray intensity $S_X \propto \delta^{4+2\alpha}$ (e.g., Marscher 1983), because of the need to calculate relevant quantities in the rest frame of the emission region. Note that the above argument does answer the question of whether the process is actually significant in a given source, because of the unknown contribution of other mechanisms to the observed flux.

Several source models could be considered, but our knowledge of the component shapes and spectra justifies only a simple model, namely a homogeneous sphere for each component (e.g., Jones, O'Dell, and Stein 1974). The fitted angular diameter depends on whether an optically thin or optically thick sphere is used. We were guided by the need for consistency with the opacities at the different frequencies indicated by the curves in Figure 8, and used a thick sphere at 5 and 11 GHz, and a thin one at 22 GHz, for component D; a thick sphere at 5 GHz and a thin sphere at 11 and 22 GHz, for component C3.

TABLE 2

COMPONENT DIAMETERS AT EPOCH 1983.10 FROM MODEL-FITTING

FREQUENCY (GHz)	COMPONENT D	COMPONENT C_3
5.0.....	(see text)	1.03 ± 0.09 thick[a]
10.7.....	0.79 ± 0.16 thick	0.94 ± 0.14 thin[b]
22.2.....	0.70 ± 0.10 thin	0.87 ± 0.10 thin

[a] Diameter of optically-thick uniform sphere.
[b] Diameter of optically-thin uniform sphere.

Table 2 gives the angular sizes with their formal errors derived from fitting sphere models, interpolated to 1983.10 from adjacent epochs at 5 and 22 GHz. Agreement between different frequencies is within the errors, which lends confidence in the sphere models, and the assumed opacities. We adopted $\theta = 0.75$ mas and $\theta = 0.95$ mas for components D and C3, respectively, for use with the X-ray formulae. At 5 GHz, the fitted sizes for component D varied greatly between epochs and had large errors, so we did not interpolate a size, as it is obviously inhomogeneous.

Published measurements of the X-ray flux density of 3C 279 made with the *Einstein* satellite during 1979 and 1980 (Zamorani *et al.* 1981; Halpern 1982; Zamorani *et al.* 1984) showed the source to be variable. The Zamorani *et al.* (1984) detections of 1979.02 and 1980.55 show a factor of 2 variation. Whether this is typical depends on how far the flux fell below the upper limits measured by Halpern. There are no published measurements closer in time to epoch 1983.10 for which we derived radio parameters. Fortunately, variations in X-ray flux density, unless very large, do not affect the calculation of the minimum allowed δ, because $\delta \propto S_X^{-r}$, where $r = 1/(4 - 2\alpha) \approx 0.17$. Likewise, relaxing the assumption of homogeneous components raises the limit on δ, which strengthens the constraints on kinematics.

The results of the X-ray computation are given in Table 3 in terms of the Doppler factor δ required to make the calculated X-ray flux agree with the observed value, which we took as

TABLE 3

MEASURED AND DERIVED SOURCE PARAMETERS

PARAMETER[a]	COMPONENT D	COMPONENT C3
ν_m (GHz).....	13.0	6.8
F_m (Jy).....	6.2	9.4
α	−1.0	−1.0
θ (mas)[b].....	0.75 ± 0.15	0.95 ± 0.15
B/δ (G).....	5.9×10^{-3}	2.9×10^{-3}
δ	1.4	3.6
Range of δ.....	0.8–2.2	2.0–6.0

[a] ν_m, F_m, α, and θ are measured quantities. B and δ are derived from limits to inverse-Compton X-ray emission; see text.
[b] Size and error determined from model-fitting homogeneous sphere.

Halpern's (1982) of $S_X = 6.6 \times 10^{-12}$ ergs s^{-1} cm^{-2} over a 0.5–4.5 keV observed energy band. This value, from epoch 1979.02, is the highest published value. The table also gives a range of possible values for δ, given the uncertainties in each parameter.

We conclude that the "jet" component C3 must be moving relativistically with respect to the quasar core ($\delta \geq 3.6$ requires a minimum Lorentz factor of $\gamma = 2$), to avoid a predicted excess of X-rays. For the core component D, the computed value of δ is consistent with unity, i.e., no bulk motion effect on the observed flux, and hence it is unlikely to dominate the emission, which perhaps suggests that the C3 dominates. However, it is entirely possible that both components have $\delta = 5$ or 10, and that the X-rays come from, say, a hot accretion disk (e.g., Begelman 1985).

d) Jets and Relativistic Beaming

Constraints on the geometry of the radio source can be deduced from the X-ray emission (§ VIc), the proper motion (§ IV), and the VLA maps. To do this, we adopt a simple model which is consistent with all the available data. The model, which is commonly used for other sources with jetlike structure, comprises two equal, oppositely directed steady streams of relativistic plasma. Knots seen on VLBI maps are assumed to be localized regions of enhanced emission, either due to shocks or instabilities, as discussed by Blandford and Königl (1979). In qualitative terms, this model explains (1) the one-sidedness of the VLBI and VLA jets, (2) the superluminal motion of the core, (3) the predicted excess of X-ray emission over the observed value, (4) the variation of spectral index with position along the jet (see Königl 1981 for a detailed discussion), and (5) the small difference in separation between the 5 and 11 GHz models. Of course, for an individual source, it is possible to adjust model parameters in an ad hoc fashion to make this model look ideal; whether it holds up in a statistical sense is still an open question (e.g., Barthel 1987). Furthermore, constraints on geometry from measurements of $\beta_{\rm obs}$ and δ, such as we discuss here, depend on the the same physical material being responsible for the beaming and the proper motion. As Aller, Hughes, and Aller (1987) have pointed out, this may be a poor assumption in real jets. Their shocked-jet model applied to 3C 279 shows the shock (i.e., the VLBI pattern) speed generally much slower than the fluid speed which yields the Doppler boosting.

For the following discussion it is convenient to consider possible jet geometries defined by β and θ as points in the ($\beta_{\rm obs}$, δ) plane, as was done by Unwin *et al.* (1983) (see their Fig. 10). In this plane, lines of constant β [or $\gamma = (1 - \beta^2)^{-1/2}$], and lines of constant θ, are orthogonal families of circles.

One critical observation is that of the jet-to-counter jet brightness ratio R, as it provides a strong constraint on the jet kinematics. It may be expressed as

$$R = \left(\frac{1 + \beta \cos \theta}{1 - \beta \cos \theta}\right)^{\eta},$$

where $\eta = 3 - \alpha$ for individual discrete components, and $\eta = 2 - \alpha$ for a continuous jet (Blandford and Königl 1979). Note that $\beta_{\rm obs}$, δ and R are all different functions of the same variables β and θ. It is easy to show that lines of constant R or $\beta \cos \theta$ are also circles in the ($\beta_{\rm obs}$, δ) plane, this time centered on the origin:

$$\beta_{\rm obs}{}^2 + \delta^2 = \frac{1 + \beta \cos \theta}{1 - \beta \cos \theta} = R^{1/\eta}.$$

Thus, a lower limit on R excludes a quadrant of the ($\beta_{\rm obs}$, δ) plane for possible jet configurations.

The limit for jet-to-counterjet ratio from the VLA maps is $R \geq 20$ (de Pater and Perley 1983), which is a better limit than can be derived from our VLBI maps, though it refers only to radii beyond 100 mas. For a measured $\alpha = -0.75$, this yields a "radius" in the ($\beta_{\rm obs}$, δ) plane of 1.49 for discrete components, and 1.72 for a continuous jet. Thus a measured R this low would be inconsistent with our value of $\beta_{\rm obs} = 2.2h^{-1}$, and lower limit $\delta > 3.6$ for component C3, which require a "radius" of 4.3, or $R \geq 50{,}000$ (≥ 3000 for a continuous jet). Therefore, the discovery of a counter jet, either on VLA or VLBI scale sizes, corresponding to a smaller value of R would be very significant, implying that at least some aspects of the simple model must be wrong.

By themselves, $\beta_{\rm obs}$ and δ provide only weak constraints on the jet geometry: $\gamma \geq 2.4$ and $\theta \leq 48°$. Since the VLBI and VLA jets are well aligned and straight, this would suggest that any foreshortening of the jet is modest.

There is already one feature which does not easily fit the model, namely the presence of a very extended and steep-spectrum ($\alpha = -0.95$) "lobe" "A" on the opposite side of the core (de Pater and Perley 1983). It is presumably nonrelativistic, and hence not Doppler-boosted, so if the arcsecond-scale jet is really double-sided, one might expect to see a lobe on the SW side as well. Another possibility is that the lobe is linked to the visible jet by some highly curved or distorted structure, though much better maps would be required to detect any emission connecting them. This may seem implausible, but in fact a link of just this kind was found in 3C 120 (Walker, Benson, and Unwin 1987), where a faint lobe was found on the opposite side of the core from the (apparently) one-sided jet. The implication in that case is that θ is so small that a modest intrinsic bend in the jet gives rise to the observed effect, i.e., the jet crosses back almost across the line of sight. As mentioned above, for 3C 279 the limit on θ is large, though it is still possible that a bend on a kiloparsec scale could be modest and still produce the observed structure. Even so, a proper understanding of the largest scales in 3C 279 must await observations of high enough dynamic range to reveal any connecting emission.

We thank the participating observatories of the US and European VLBI Networks for their contributions to the observations presented here, and we thank the many individuals involved in scheduling, observing, and data reduction. In particular we are grateful to colleagues at southern hemisphere observatories who provided VLBI data: Dr. G. Nicolson of the Hartebeesthoek Radio Observatory, South Africa; and Dr. P. Kaufmann of the Instituto de Pesquisas Espaciais, Brazil. The telescopes at Haystack, NRAO, VLA, Fort Davis, OVRO, and Hat Creek are supported, in part, by the National Science Foundation. This work was supported by NSF grant AST85-09822 to the Owens Valley Radio Observatory.

REFERENCES

Aller, H. D. 1970, *Ap. J.*, **161**, 19.
Aller, H. D., Aller, M. F., Latimer, G. G., and Hodge, P. E. 1985, *Ap. J. Suppl.*, **59**, 513.
Aller, H. D., Hughes, P. A., and Aller, M. F. 1987, in *Superluminal Radio Sources*, ed. J. A. Zensus and T. J. Pearson (Cambridge: Cambridge University Press), p. 273.

Aller, H. D., and Olsen, E. T. 1971, *A.J.*, **76**, 671.
Andrew, B. H., Macleod, J. M., Harvey, G. A., and Medd, W. J. 1978, *A.J.*, **83**, 863.
Barthel, P. D. 1987, in *Superluminal Radio Sources*, ed. J. A. Zensus and T. J. Pearson (Cambridge: Cambridge University Press), p. 148.
Begelman, M. C. 1985, in *Astrophysics of Active Galaxies and Quasi-Stellar Objects*, ed. J. S. Miller (Mill Valley: University Science Books), p. 411.
Biretta, J. A., *et al.* 1985, *Ap. J. (Letters)*, **292**, L5.
Biretta, J. A., Moore, R. L., and Cohen, M. H. 1986, *Ap. J.*, **308**, 93.
Blandford, R. D. 1987, in *Superluminal Radio Sources*, ed. J. A. Zensus and T. J. Pearson (Cambridge: Cambridge University Press), p. 310.
Blandford, R. D., and Königl, A. 1979, *Ap. J.*, **232**, 34.
Burbidge, E. M., and Rosenburg, F. D. 1965, *Ap. J.*, **142**, 1673.
Cohen, M. H., *et al.* 1975, *Ap. J.*, **201**, 249.
Cornwell, T. J., and Wilkinson, P. N. 1981, *M.N.R.A.S.*, **196**, 1067.
Cotton, W. D., *et al.* 1979, *Ap. J. (Letters)*, **229**, L115.
de Pater, I., and Perley, R. A. 1983, *Ap. J.*, **273**, 64.
Haddock, T. F., Aller, H. D., and Aller, M. F. 1987, *A.J.*, **93**, 1356.
Halpern, J. 1982, Ph.D. thesis, Columbia University.
Hughes, P. A., Aller, H. D., and Aller, M. F. 1986, *Ap. J.*, **298**, 301.
———. 1989, *Ap. J.*, **341**, in press.
Jones, T. W., O'Dell, S. L., and Stein, W. A. 1974, *Ap. J.*, **192**, 261.
Königl, A. 1981, *Ap. J.*, **243**, 700.
Landau, R., *et al.* 1986, *Ap. J.*, **308**, 78.
Marscher, A. P. 1983, *Ap. J.*, **264**, 296.
Miley, G. K. 1971, *M.N.R.A.S.*, **152**, 477.
Moore, R. L., and Stockman, H. S. 1981, *Ap. J.*, **243**, 60.
Mutel, R. L., and Phillips, R. B. 1987, in *Superluminal Radio Sources*, ed. J. A. Zensus and T. J. Pearson (Cambridge: Cambridge University Press), p. 60.
Padrielli, L., *et al.* 1987, *Astr. Ap. Suppl.*, **67**, 63.
Pauliny-Toth, I. I. K., Preuss, E., Witzel, A., Graham, D., Kellerman, K. I., and Rönnäng, B. 1981, *A.J.*, **86**, 371.
Pauliny-Toth, I. I. K., Wade, C. M., and Heeschen, D. S. 1966, *Ap. J. Suppl.*, **116**, 65.
Pilbratt, G. 1986, Ph.D. thesis, Chalmers University of Technology, Göteburg, Sweden.
Pilkington, J. D. H., and Scott, P. F. 1965, *Mem. R.A.S.*, **69**, 183.
Roellig, T. L., Becklin, E. E., Impey, C. D., and Werner, M. W. 1986, *Ap. J.*, **304**, 646.
Roberts, D. H., and Wardle, J. F. C. 1987, in *Superluminal Radio Sources*, ed. J. A. Zensus and T. J. Pearson (Cambridge: Cambridge University Press), p. 193.
Salonen, E., *et al.* 1987, *Astr. Ap. Suppl.*, **70**, 409.
Schwab, F. R., and Cotton, W. D. 1983, *A.J.*, **88**, 688.
Seielstad, G. A., Pearson, T. J., and Readhead, A. C. S. 1983, *Pub. A.S.P.*, **95**, 842.
Slee, O. B. 1977, *Australian J. Phys. Suppl.*, **43**, 1.
Slee, O. B., and Higgins, C. S. 1973, *Australian J. Phys. Suppl.*, **23**, 1.
Unwin, S. C. 1987, in *Superluminal Radio Sources*, ed. J. A. Zensus and T. J. Pearson (Cambridge: Cambridge University Press), p. 34.
Unwin, S. C., Cohen, M. H., Biretta, J. A., Pearson, T. J., Seielstad, G. A., Walker, R. C., Simon, R. S., and Linfield, R. P. 1985, *Ap. J.*, **289**, 109.
Unwin, S. C., Cohen, M. H., Pearson, T. J., Seielstad, G. A., Simon, R. S., Linfield, R. P., and Walker R. C. 1983, *Ap. J.*, **271**, 536.
Vetukhnovskaya, Y. N. 1987, *Pis'ma Astron. Zh.*, **13**, 376; (Engl. trans. in 1987, *Soviet Astr. Letters*, **13**, 154).
Walker, R. C., Benson, J. M., and Unwin, S. C. 1987, *Ap. J.*, **316**, 546.
Whitney, A. R., *et al.* 1971, *Science*, **173**, 225.
Wills, B. J. 1975, *Australian J. Phys. Suppl.*, **38**, 1.
Zamorani, G., *et al.* 1981, *Ap. J.*, **245**, 357.
Zamorani, G., Giommi, P., Maccacaro, T., and Tananbaum, H. 1984, *Ap. J.*, **278**, 28.

J. A. Biretta: Harvard-Smithsonian Center for Astrophysics, 60 Garden Street, Cambridge, MA 02138

M. H. Cohen, S. C. Unwin, and J. A. Zensus: Owens Valley Radio Observatory, California Institute of Technology, Mail Code 105-24, Pasadena, CA 91125

M. W. Hodges: Owens Valley Radio Observatory, Box 968, Big Pine, CA 93513